Comparison of the crystalline structure, morphology, and magnetic properties of γ-phase $Mn/Cu_3Au(100)$ ultrathin films by varying the growth temperature

W. C. Lin,[1,2] T. Y. Chen,[1,2] L. C. Lin,[1] B. Y. Wang,[1,2] Y. W. Liao,[1,2] Ker-Jar Song,[2] and Minn-Tsong Lin[1,2,*]
[1]*Department of Physics, National Taiwan University, Taipei 10617, Taiwan*
[2]*Institute of Atomic and Molecular Sciences, Academia Sinica, 10617 Taipei, Taiwan*
(Received 12 May 2006; revised manuscript received 22 December 2006; published 23 February 2007)

The structural and magnetic properties of room-temperature (RT: 300 K)-grown and low-temperature (LT: 100 K)-grown $Mn/Cu_3Au(100)$ thin films were investigated. Mn films deposited at RT and LT demonstrate very different behaviors in the crystalline structure, morphology, and magnetism. RT-Mn films reveal apparent layer-by-layer growth for 0–2 ML (monolayer) followed by reduced oscillations. Although the medium-energy electron diffraction (MEED) oscillation is reduced, the intensity of specular spot increases monotonically after 6–7 ML, inferring the tendency of smooth morphology. The study of scanning tunneling microscopy also shows that even in 19 ML $Mn/Cu_3Au(100)$, the surface morphology is composed of large terraces with the size up to hundreds of nanometers. The LT-Mn films reveal apparent layer-by-layer growth for 0–5 ML followed by the reduced oscillations, and then the MEED intensity remains at low intensity, inferring the rough surface. The RT- and LT-Mn films exhibit a thickness-dependent structural transition from a face-centered cubic to a face-centered tetragonal structure at different critical thicknesses, ~12–14 and ~8 ML, respectively. Significant exchange bias is observed in Fe/RT-Mn bilayers. It increases monotonously with Mn thickness. The exchange bias coupling in Fe/LT-Mn is much weaker than Fe/RT-Mn and drastically varies with Mn film thickness. The presence of exchange bias in the Fe/Mn bilayers also indicates the antiferromagnetism of γ-phase $Mn/Cu_3Au(100)$.

DOI: 10.1103/PhysRevB.75.054419 PACS number(s): 75.70.Ak, 75.50.Bb, 78.20.Ls

I. INTRODUCTION

Bulk Mn exhibits complicated structural transitions at various temperatures. α-phase (58 atoms per cubic cell) Mn is stable below 1000 K,[1] revealing antiferromagnetic (AFM) ordering with the phase transition temperature $(T_N) < 100$ K. β-phase (20 atoms per cubic cell), γ-phase [face-centered cubic (fcc)], and δ-phase [body-centered cubic (bcc)] Mn also sequentially appear at the temperatures higher than 1000 K. Due to the high temperature, the magnetic ground states of bulk Mn materials with the above structures are unable to be characterized. How to prepare Mn samples with stable fcc or bcc structure near room temperature thus becomes an important issue. About 30 years ago, the γ-phase bulk Mn samples were prepared by rapid quenching of Mn with dilute concentration of Cu, Ni, Pd, or Fe, revealing the AFM ordering with $T_N = 540$ K.[2] However, since the last decade, the pure γ- and δ-phase Mn films are prepared by epitaxial growth on single-crystalline substrates such as Cu(100),[3–5] Fe(100),[6] and Ag(100),[7] etc. Due to the complexity and variety in the structure of Mn materials, the magnetic properties of Mn with different structures still attract many theoretical[8–11] and experimental[3,4,6,7,12,13] efforts up to now. In recent studies,[12,13] Mn ultrathin films grown on $Cu_3Au(100)$ substrate at room temperature reveal the well-defined γ-phase crystalline structure. A transition from a fcc to a face-centered tetragonal (fct) structure is also observed with film thickness.[12,13] By capping the Fe overlayer, the AFM properties of γ-Mn films can be detected through the exchange bias coupling in the Fe/Mn bilayers.[13] However, so far studies on the interrelation between the crystalline structure, surface morphology, and magnetism in such γ-Mn films are still absent.

Experimentally, the growth temperature possesses crucial effects on the crystalline structure, morphology, and the magnetic properties of thin films. In general, growth at low temperature (LT) highly enhances the surface roughness with increasing thickness. Usually, the magnetic properties including the surface anisotropy, crystalline anisotropy, etc., are strongly dependent on the surface morphology and crystalline structure. Thus, the magnetic behavior of ultrathin films can be affected by the growth temperature seriously. For example, $Fe/Cu_3Au(100)$ (Refs. 14 and 15) films reveal a fcc to bcc structural transition and simultaneously the perpendicular to in-plane spin-reorientation transition at the critical thicknesses of 3.5 and 5.5 ML (monolayer) for room-temperature (RT) and LT growths, respectively. Similar instances of the crucial effects induced by variation of growth temperature are also reported in Ni/Cu(100),[16] Fe/Cu(100),[17] $Ni/Cu_3Au(100)$,[18] Co/Cu(100),[19,20] etc. Since varying the growth temperature might result in significant differences in the crystalline structure, morphology, and magnetic properties, the comparison on the γ-phase Mn films grown at LT and RT can be a good way for clarifying their interrelation. Thus, in this study, the systematic comparison between the RT-grown and the LT-grown films in various aspects is made. The correlations between the crystalline structure, surface morphology, and magnetic properties in the γ-Mn thin films are also discussed.

II. EXPERIMENT

The thin-film preparation and measurements were carried out in a multifunctional ultrahigh-vacuum chamber with the base pressure better than 2×10^{-10} torr. After cycles of

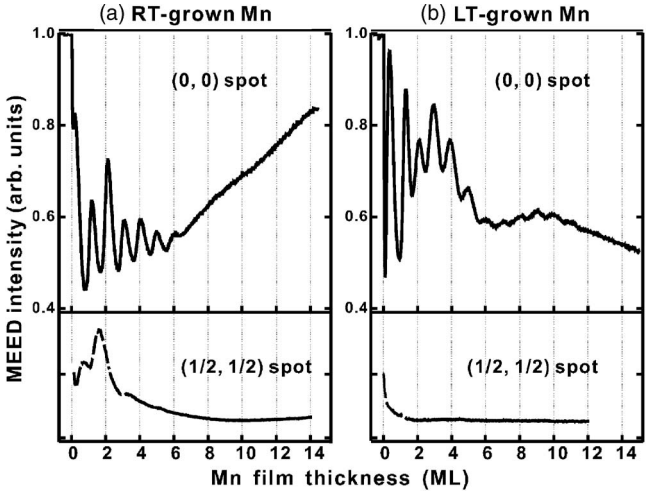

FIG. 1. Recorded intensity of MEED (0 0) and $(\frac{1}{2}\frac{1}{2})$ spots for Mn films grown on $Cu_3Au(100)$ at RT and LT.

3 keV Ne^+ sputtering and annealing, the clean substrate of $Cu_3Au(100)$ with well-ordered $c(2\times2)$ superstructure and flat surface was obtained.[21] Mn was evaporated onto the substrate with the substrate temperatures of 300 K (RT) and 100 K (LT). During the evaporation, the pressure was better than 4×10^{-10} torr and the growth was monitored by medium-energy electron diffraction (MEED) with the beam energy of 5 keV and the grazing angle of 1°. From the periodicity of MEED oscillations, the deposition rate was calibrated precisely. The LT-grown Mn films were annealed to 300 K for 5 min right after the deposition, so that the LT- and RT-grown films underwent the same annealing processes. A 21 ML Fe layer was sequentially deposited over the $Mn/Cu_3Au(100)$films at RT.

The morphology of RT-grown Mn films was characterized by scanning tunneling microscope (STM). Due to the limited instruments, STM study of LT-Mn was not performed here. The STM images shown in the text were taken under the constant current mode at RT. The lateral crystalline structure was characterized at 100 K by low-energy electron diffraction (LEED). In this experiment, a spot-profile-analysis-LEED was used to take the LEED images. Besides, from the LEED-I/V curves, the average vertical interlayer distance ($d_\perp$) of the film was determined using the kinetic approximation.[21,22] Magnetic properties of the films were detected by magneto-optical Kerr effect (MOKE). The MOKE measurement was performed in both in-plane and perpendicular geometries with the modulation and lock-in technique. All the MOKE measurements of Fe/Mn bilayers were performed after a field-cooling process from 300 to 100 K under an in-plane magnetic field of 1000 Oe along the [001] direction.

III. RESULTS

A. Growth of RT-Mn/$Cu_3Au(100)$ and LT-Mn/$Cu_3Au(100)$

Figure 1 shows the MEED intensities of (0 0) and $(\frac{1}{2}\frac{1}{2})$ spots for RT-grown and LT-grown Mn films. In Fig. 1(a), Mn grown on $Cu_3Au(100)$ at RT reveals apparent layer-by-layer growth for 0–2 ML. After 2 ML, the oscillation amplitude is reduced and then gradually disappears after 6–7 ML. Interestingly, although the MEED oscillation amplitude is reduced with film thickness, the intensity of specular spot increases monotonically after 6–7 ML. It inhibits the tendency of smooth surface morphology with increasing film thickness. The STM studies shown later also prove the inference. Even in 19 ML $Mn/Cu_3Au(100)$, the surface morphology is composed of the large terraces with size up to several hundred nanometers. In contrast, the LT-grown films reveal apparent layer-by-layer growth for 0–5 ML followed by the reduced oscillations. Unlike the monotonic increase of the (0 0) spot intensity in RT-grown films after 6–7 ML, the (0 0) spot intensity of LT-grown films significantly decreases after ~10 ML, indicating the rough surface morphology for LT-Mn at higher thickness. That also might be why we get such dramatic changes in H_c and H_e after ~10 ML, which will be discussed later in the text.

The period of the first peak for LT-Mn film is much less than 1 ML. After 2 ML, each peak regularly matches the integer layers until the disappearance of oscillation. The unique peak always repeats in LT-Mn films. The shoulder in RT-Mn MEED for 0–1 ML also repeats in each preparation. Something seems to happen for 0–1 ML for LT- and RT-Mn films. It might be due to some alloy effect or structural variation at the interface, but it is still unclear to us. Further LEED or STM work is needed for the detailed mechanism, which is beyond the content of this paper.

The MEED oscillation in Fig. 1 is different from the previous study by Schirmer *et al.*[12] The possible reasons might be the following. (1) The different MEED geometries: in our MEED geometry, the grazing angle=1° and the beam energy=5 keV. In the previous study,[12] the grazing angle =8.6° and the beam energy=3 keV. These differences might affect the oscillation curves seriously. For example, in the $Ni/Cu_3Au(100)$ system,[21,23] the different MEED geometries do result in obvious differences in the MEED curves. (2) The different deposition conditions of Mn, such as deposition rate, direction, etc.: some reports have already shown that these parameters can affect the thin-film growth seriously.[24] The reason may be quite complicated and need further detailed studies. Basically the trends of MEED curves in our study and the previous study[12] are quite similar: the intensity increases for RT growth and decreases for LT growth with film thickness. The trend of MEED intensity roughly indicates the roughness condition, which is also confirmed by STM to be consistent in this work in RT-Mn films. The crystalline structures of our work and the previous study are also consistent, as shown later in the text. The most distinct differences are the number and amplitude of MEED oscillations. The latter is supposed to be quite sensitive to the e-beam energy and grazing angle.

The initial intensity of MEED $(\frac{1}{2}\frac{1}{2})$ spot denotes the $c(2\times2)$ structure of $Cu_3Au(100)$. In general, the $(\frac{1}{2}\frac{1}{2})$ spot disappears after the deposition of 1–2 ML film, just like the case of LT-grown Mn shown in Fig. 1(b). The first and the second ML LT-grown Mn cover the original $c(2\times2)$ structure of $Cu_3Au(100)$. For the RT-grown Mn, the intensity of

the $(\frac{1}{2}\frac{1}{2})$ spot, instead of drastically diminishing right after deposition, oscillates with film thickness with the local maxima at 0.5 and 1.5 ML and becomes invisible after ~6 ML. The presence of the $(\frac{1}{2}\frac{1}{2})$ spot for RT-grown Mn films at such high thickness indicates the formation of an additional ordered structure on the surface. There are two possibilities for the ordered structure. It might just come from the reconstruction of Mn surface itself. Besides, from the comparison on the Auger signal as a function of Mn thickness in RT- and LT-Mn/$Cu_3Au(100)$ films, the disappearance of Au Auger signal (at 69 eV) with increasing Mn thickness is delayed by ~2 ML in RT-Mn films as compared with LT-Mn films. This result indicates the Au segregation in the first few monolayers for the RT-grown Mn films. In the previous studies of Co-Ni/$Cu_3Au(100)$ alloy films,[18,21,25] similar results of Au segregation have also been reported. Thus, the Au segregation might be another reason for the presence of superstructure. Besides, in the previous study of Mn/$Cu_3Au(100)$,[12] the critical annealing temperatures for Cu- and Au segregation are nearly the same, indicating similar behavior of interdiffusion at Mn/Cu_3Au interface. Our Auger electron spectroscopy (AES) data reveal that ~10 ML Mn film is enough to cover the Cu signal. This result as well as the previous study on Mn/$Cu_3Au(100)$ (Ref. 12) also demonstrate the limited interdiffusion at the Mn/Cu_3Au interface. In other words, significant Mn-Cu-Au alloying may extend to only 1–2 ML near the interface. The possibilities of the interface alloy effect on the crystalline structure and magnetic behavior will be discussed later in the text.

B. Structures of RT-Mn/$Cu_3Au(100)$ and LT-Mn/$Cu_3Au(100)$

Figure 2 shows the LEED patterns of $Cu_3Au(100)$ and various Mn films grown at RT and LT. Figure 2(a) exhibits the $c(2\times2)$ structure of $Cu_3Au(100)$. From the presence of the MEED $(\frac{1}{2}\frac{1}{2})$ spot, 0–6 ML RT-Mn films are supposed to reveal superstructure on the surface. In more detail, as shown in Fig. 2, 0.5 and 1 ML RT-Mn films reveal $p(2\times2)$ structure. For 5 ML, a transition to $c(2\times2)$ structure is observed. With the larger coverage of more than ~9 ML, the RT-Mn films always reveal the $p(1\times1)$ LEED pattern. Moreover, as shown in Figs. 2(e)–2(h), the LEED spot profile of 9.2–11.5 ML RT-Mn is apparently broader than that of 17–24.5 ML films. This observation indicates two possibilities for the difference. There might be a structural transition or some significant variation in morphology between 11.5 and 17 ML RT-Mn. In the following sections, the studies of LEED-I/V and STM indeed show that both of the two suggestions truly happen. The sharp $p(1\times1)$ LEED pattern in Fig. 2(h) indicates the well-ordered crystalline structure and coherent growth of RT-grown Mn on $Cu_3Au(100)$ up to ~24 ML.

Since the MEED $(\frac{1}{2}\frac{1}{2})$ spot intensity is drastically reduced right after the deposition at LT, the LT-grown Mn films always reveal a $p(1\times1)$ LEED pattern as shown in Fig. 2. The LEED spots become sharper for 8.3–13.3 ML. Afterward, the spot intensity gets more and more unclear with thickness. For the quantitative analysis, the LEED line profiles normalized by the background are shown in Fig. 3. The consistent peak positions indicate the coherent growth throughout the investigated thickness region. RT-Mn exhibits sharp LEED spots and a high ratio of peak intensity to background even in high coverages. In contrast, LT-Mn exhibits sharp spots around ~13 ML, after which the peak intensity gradually decreases. The thickness-dependent evolution of LEED data suggests the possibilities of the structural transition and the variation in surface morphology, which are, as discussed later, also strongly correlated to the exchange bias behavior in the Fe/Mn bilayers.

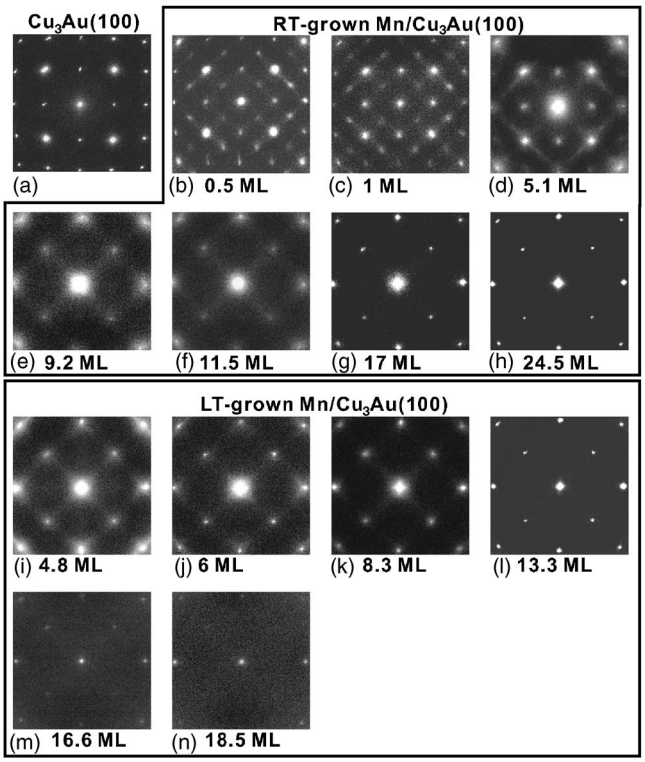

FIG. 2. LEED images of the RT- and LT-grown Mn/$Cu_3Au(100)$ films with different thicknesses. All the images are taken at 100 K with the beam energy=150 eV.

Besides the LEED images, the LEED-I/V curves of specular spot are also recorded for the analysis of interlayer distance $(d_\perp)$.[13] Figure 4 shows the LEED-I/V curves of LT-grown Mn films. The LEED-I/V curves of RT-grown Mn films have been reported in our previous studies.[13] The integers denote the orders of the maximum conditions in Bragg interference. The indexed peak positions shift toward high energy both in RT- and LT-Mn films with increasing thickness. The shift toward high energy indicates a structural transition toward the smaller $d_\perp$. Figure 5 shows the $d_\perp$ deduced from the LEED-I/V curves. Mn films with low coverage reveal a $d_\perp$ almost the same as that of the substrate $Cu_3Au(100)$. At a higher thickness, the $d_\perp$ is reduced to about 1.77 Å. Since the LEED studies inform the coherence growth of Mn on $Cu_3Au(100)$, the Mn films are concluded to perform a structural transition from a fcc to a fct structure with the c/a ratio ~95%. The gray regions in Fig. 5 indicate the critical thicknesses for the structural transition. For the RT- and LT-grown Mn films, the critical thicknesses are ~12–14 and ~8 ML, respectively.

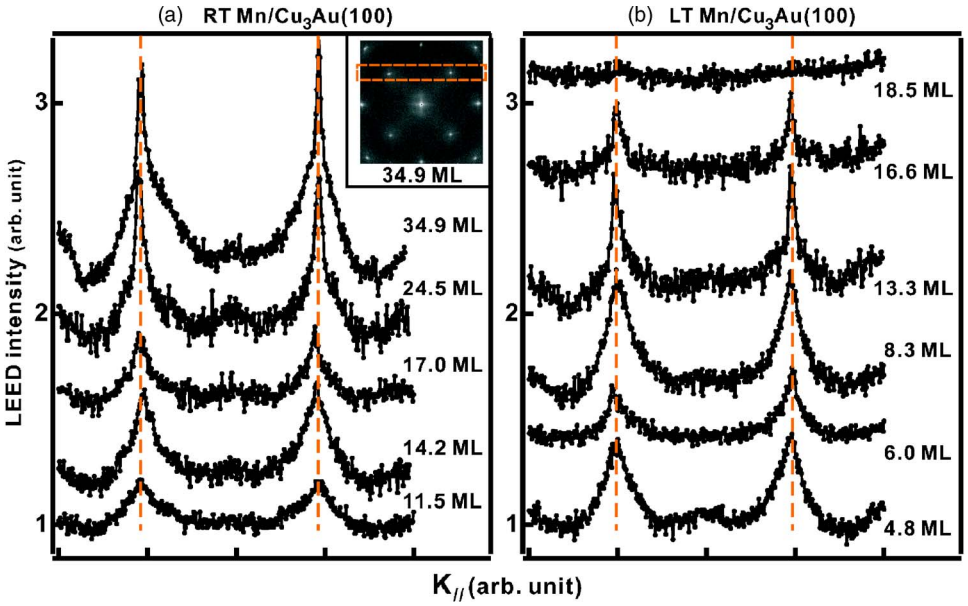

FIG. 3. (Color online) Line profile analysis of the LEED patterns shown in Fig. 2. The inset in (a) indicates the position of the line profile.

C. Morphology of RT-Mn/Cu_3Au(100)

In the above sections, for the RT-Mn, the recorded MEED intensity implicates the smoother surface with increasing thickness, and the LEED-*I*/*V* analysis also indicates a structural transition from fcc to fct at ~12–14 ML. The morphology evolution with film thickness for RT-Mn will be an interesting issue and might be strongly correlated to the MEED and LEED results. Figure 6 shows the STM images of RT-grown Mn/Cu_3Au(100) films with various thicknesses. The insets in Figs. 6(a)–6(e) and 6(g) exhibit the line profile at the solid lines in each images. In Figs. 6(a)–6(c), the RT-Mn reveal atomically flat surface with small two-dimensional (2D) islands of single atomic height. This observation is consistent with the layer-by-layer growth indicated by MEED oscillation. For the films with a higher coverage [Figs. 6(d) and 6(e)], no further 2D islands are observable. The surface is composed of elongated terraces and multisteps. Furthermore, a clear plaid pattern is observed on the surface. Figures 6(f)–6(h) show the morphology of 19 ML RT-grown Mn/Cu_3Au(100) in different scales. The terraces become very large with the size up to several hundred nanometers and the shape is no longer elongate [Fig. 6(f)]. The plaid pattern still exists on the surface for 19 ML RT-Mn and the corrugation is less than 1 Å [Fig. 6(g)]. In more detail, the edge of the rectangularlike units in the plaid

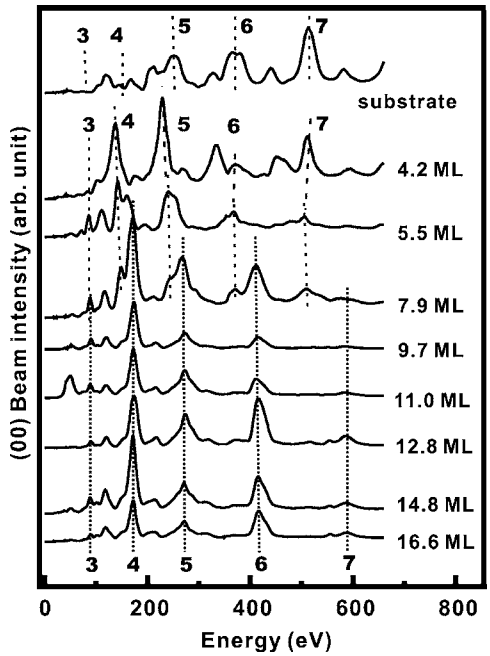

FIG. 4. LEED-*I*/*V* curves of various LT-grown Mn/Cu_3Au(100) films with different thicknesses measured at 100 K. The integers denote the orders of the maximum conditions in Bragg interference.

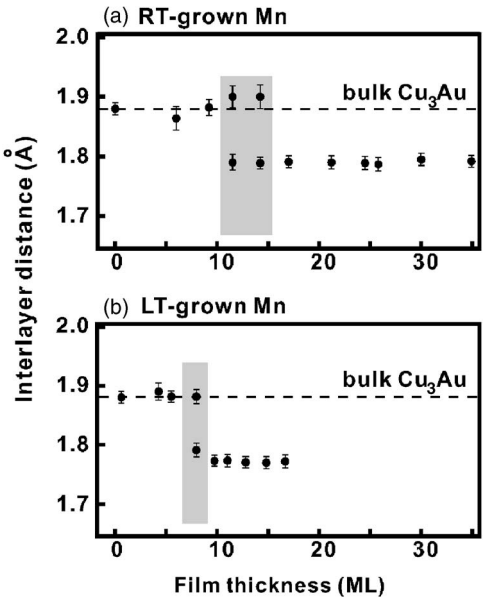

FIG. 5. The solid circles indicate the interlayer distances of various (a) RT-grown and (b) LT-grown Mn/Cu_3Au(100) films with different thicknesses measured at 100 K. The dotted line indicates the interlayer distance of Cu_3Au(100).

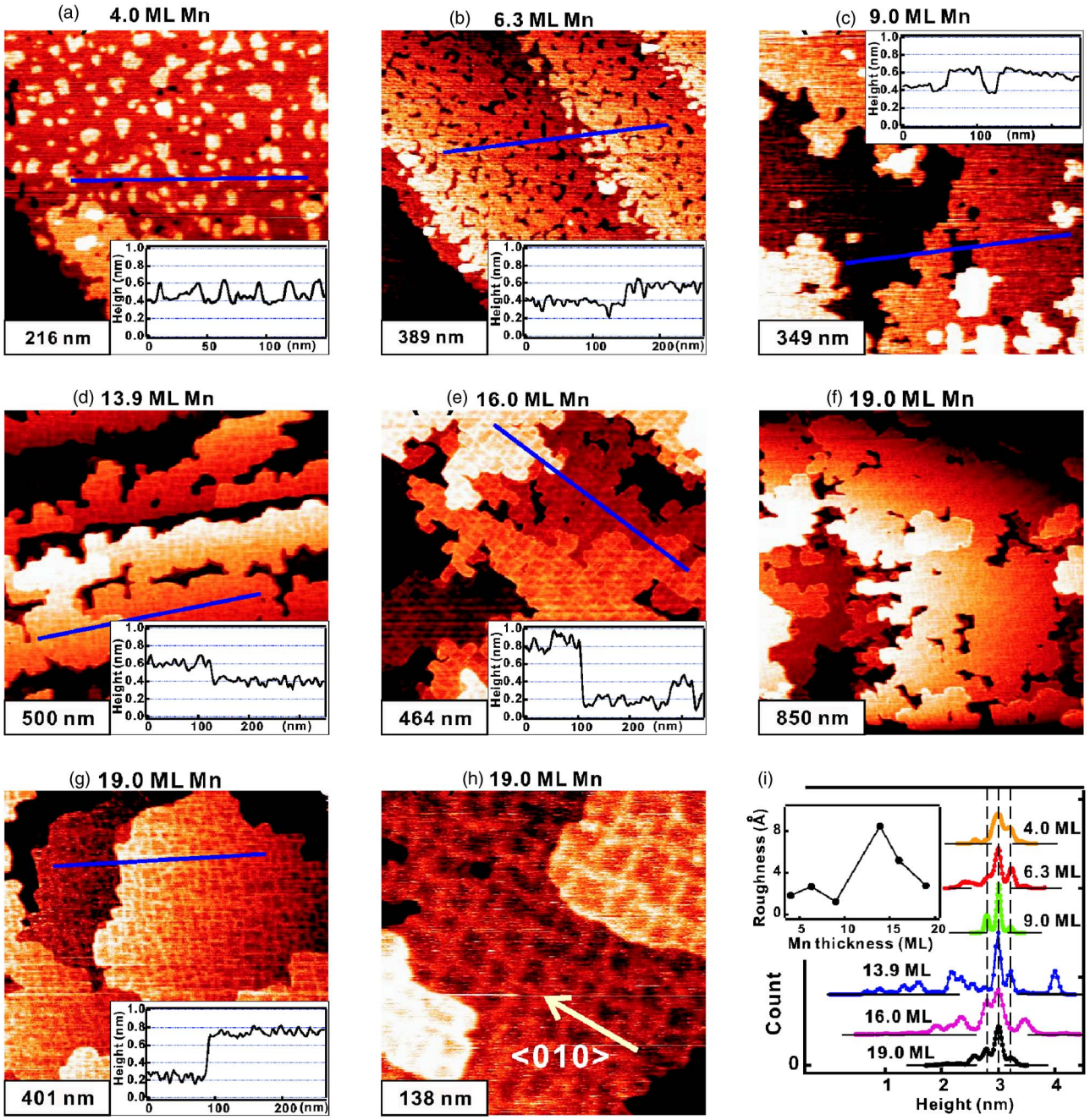

FIG. 6. (Color online) STM images of various RT-grown $Mn/Cu_3Au(100)$ with different thicknesses. These STM images were taken under the constant current mode at RT with the following tunneling currents and bias voltages: (a) 0.9 V, 1.2 nA; (b) −1.8 V, 0.8 nA; (c) 1.3 V, 0.8 nA; (d) 1.8 V, 0.8 nA; (e) 1.8 V, 1.0 nA; (f) 1.5 V, 1.5 nA; (g) 1.5 V, 1.5 nA; and (h) 0.8 V, 1.5 nA. Since the $Mn/Cu_3Au(100)$ is a good conducting sample, the variations of the bias voltage and tunneling current do not cause significant differences on the scanning results. (i) Roughness and histogram of the above STM images: (a)–(e) and (g).

pattern is about 10–20 nm and aligns roughly along the ⟨001⟩ directions. The grid lines of the pattern in different terraces follow and continue even across the step [Fig. 6(h)]. Unlike the morphology of 4–9 ML RT-Mn [Figs. 6(a)–6(c)], there are no more 2D islands on the surface with the coverage up to 19 ML. Although the MEED oscillation ceases after 6 ML, the intensity of specular spot keeps on increasing, and the STM studies also prove the smooth surface composed of large terraces. The above observations also suggest the possibility of step-flow-growth of the RT-grown Mn films on $Cu_3Au(100)$.

Figure 6(i) reveals the roughness and histogram of the STM images: Figs. 6(a)–6(e) and 6(g). The roughness analyzed as a function of Mn thickness is qualitatively consistent with the MEED curve in Fig. 1(a): the roughness initially increases (at 13.9 ML) and then goes back to a smooth surface (at 19 ML). More STM images will be needed for the quantitative statistics. Besides, from the histogram analy-

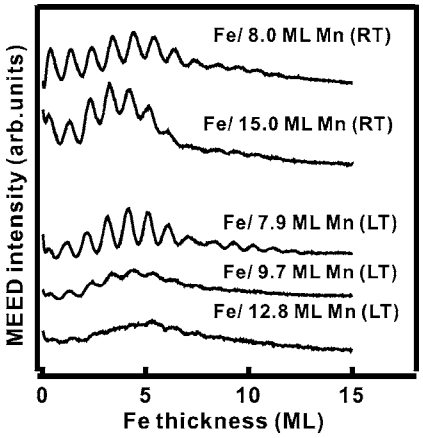

FIG. 7. Recorded intensity of MEED specular spot for Fe films deposited on various RT-Mn/$Cu_3Au(100)$ and LT-Mn/$Cu_3Au(100)$ films. All the Fe films were deposited with the substrate temperature at RT.

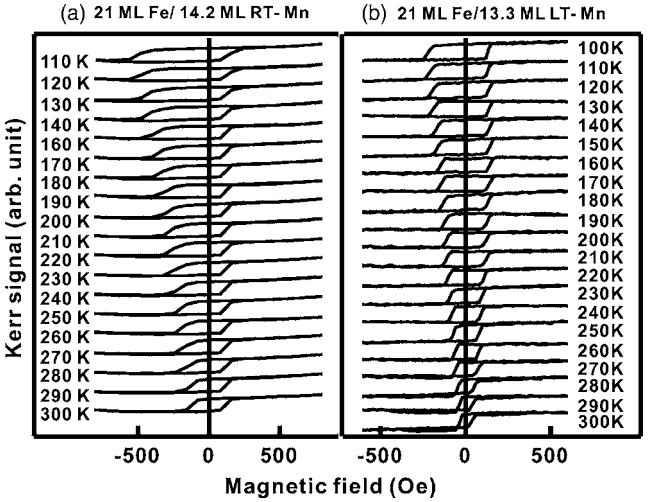

FIG. 8. MOKE hysteresis loops of (a) 21 ML Fe/14.2 ML RT-grown Mn/$Cu_3Au(100)$ and (b) 21 ML Fe/13.3 ML LT-grown Mn/$Cu_3Au(100)$ measured with increasing temperatures after a field-cooling process from RT to 100 K under a 1000 Oe magnetic field along the [001] direction.

sis, the discrete peaks indicate the layerwise structure in surface morphology. In this case of RT-Mn films, for 13.9–16 ML, the roughness is increased by extending the range of height distribution, but meanwhile keeping the atomic terraces with the size ≈ tens to hundreds of nanometers.

D. Growth of Fe films on RT-Mn/$Cu_3Au(100)$ and LT-Mn/$Cu_3Au(100)$

Since there are no hysteresis loops observed in polar and longitudinal geometries at 300–100 K, the Mn films are suspected to be antiferromagnetic (AFM). 21 ML Fe films are deposited on the RT- and LT-grown Mn films in order to detect the possible AFM properties of these Mn films through the FM/AFM exchange bias coupling. Figure 7 shows the MEED oscillation of Fe films deposited on various RT- and LT-Mn films. For Fe/8 ML and 15 ML RT-Mn, the MEED oscillations reveal nearly the same features: apparent layer-by-layer growth sustains up to 6–7 ML and then gradually disappears. However, for Fe grown on LT-Mn, the MEED oscillations become more and more faint with increasing Mn thickness. This effect is ascribed to the evolution of surface roughness in the LT-Mn. From the monotonic decrease of the MEED intensity after ~5 ML [Fig. 1(b)], the LT-Mn films should reveal the rougher surface morphology with increasing thickness, which results in the disappearance of the layer-by-layer growth for the Fe overlayer. In contrast to LT-Mn, the flat surface morphology of RT-Mn with various thicknesses still promises the layer-by-layer growth of the Fe overlayer. It is worth noticing that the consistent results of Figs. 1 and 7 point out the clear contrast of the smooth surface for RT-Mn to the rough surface for LT-Mn films at a high thickness.

E. Magnetic properties of 21 ML Fe/RT-Mn/$Cu_3Au(100)$ and 21 ML Fe/LT-Mn/$Cu_3Au(100)$

In order to detect the AFM properties of Mn films, the 21 ML Fe layer is deposited on the Mn films. The 21 ML Fe layer is characterized to be always of body-centered-cubic structure with in-plane easy axis along the ⟨001⟩ directions.[14,15] After a field-cooling process from 300 to 100 K under an in-plane magnetic field of 1000 Oe, the exchange bias coupling in the FM Fe/AFM Mn bilayers is investigated by MOKE. The investigation of exchange bias coupling indicates the AFM properties of Mn films. Figure 8 gives two examples of the temperature-dependent MOKE hysteresis loops for Fe/RT- and Fe/LT-grown Mn bilayers. At ~100 K, the apparent shift of MOKE hysteresis loops is observed for both Fe/RT-Mn and Fe/LT-Mn. In Fig. 8(a), 21 ML Fe/14.2 ML RT-Mn bilayer reveals an exchange bias of 180 Oe at 110 K with the blocking temperature (T_b) up to 290 K. However, for 21 ML Fe/13.3 ML LT-Mn bilayer, as shown in Fig. 8(b), an exchange bias of only 40 Oe was measured at 110 K with T_b=170 K. Since there is only very limited difference between the Mn coverage of the above two cases, the exchange bias coupling in Fe/LT-Mn bilayers is concluded to be much weaker than that in Fe/RT-Mn. Both the MEED oscillations of Mn on $Cu_3Au(100)$ (Fig. 1) and Fe on Mn/$Cu_3Au(100)$ (Fig. 7) indicate the rougher surface of LT-grown Mn than RT-Mn after ~10 ML. Thus, the roughness in the Fe/Mn interface might be the origin of the significant difference in the exchange bias properties.

The existence of the exchange bias field strongly suggests the antiferromagnetism of the γ-phase Mn films. Besides the AFM Mn films, there are other two possible origins of the AFM phase which may induce the exchange bias: (1) Near the Fe/Mn interface, there might be a few monolayers of residual fcc Fe which is predicted to be AFM in some theoretical calculations. (2) The Fe-Mn alloy formed at the interface might be AFM in certain composition.

Figure 9(b) shows the AES ratio of Mn-542 eV/Fe-703 eV as a function of Fe thickness in n ML Fe/10 ML Mn. Apparently, the AES ratio decays to <0.2 after 7–8 ML Fe. The residual AES ratio of ~0.2 is due to

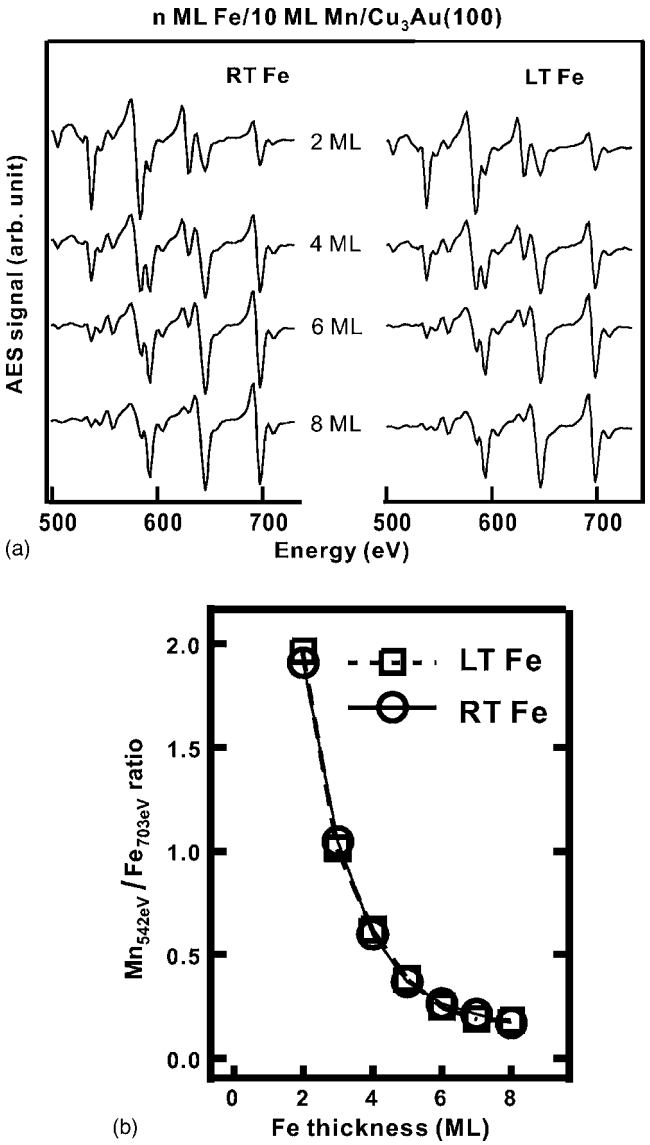

FIG. 9. (a) Auger spectra of RT- and LT-grown Fe films on 10 ML RT-Mn/$Cu_3Au(100)$. (b) Auger ratio of Mn-542 eV/Fe-703 eV as functions of Fe film thickness. The AES data conclusively exclude the possibility of serious alloy formation at the Fe/Mn interface.

the small Fe peaks around 542 eV, not the residual Mn-542 eV signal [see the spectra in Fig. 9(a)]. Since LT-growth can reduce the interdiffusion at the interface, the comparison between RT-Fe/Mn and LT-Fe/Mn can help tell if the RT-Fe/Mn have serious interdiffusion. As shown in Fig. 9(b), the decay rates of RT-Fe/Mn and LT-Fe/Mn are nearly the same, indicating the same condition at the interface. Although the AES data in Fig. 9 cannot exactly exclude the possibility of 1–2 ML FeMn alloy at the interface, it can still exclude the possibility of serious alloy formation (for example, >4–5 ML FeMn) at the interface. In the atomically and chemically resolved STM studies on Mn/Fe(001), grown at 370 K by Yamada *et al.*,[26] Fe atoms intermix with the first (14%), the second (4%), and the third Mn layer (2%), while a negligible amount of Fe atoms is found above

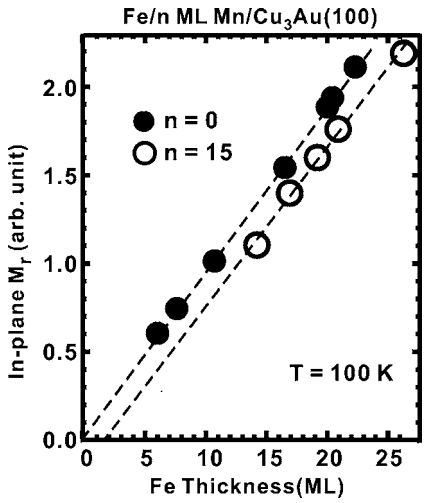

FIG. 10. The remanent MOKE signal (M_r), which is also the saturation signal due to the square loops, of n ML Fe on $Cu_3Au(100)$ and 15 ML Mn/$Cu_3Au(100)$. All the Fe films are deposited with the substrate temperature at RT. The dead layer of Fe on Mn/$Cu_3Au(100)$ is only about ~2 ML due to the intermixing at Fe/Mn interface, which is consistent with the AES data in Fig. 8. The absence of M_r for 0–12 ML Fe on 15 ML Mn/$Cu_3Au(100)$ is due to the exchange-bias-induced very large coercivity field, which is beyond the accessible range of our magnetic field.

the third layer. This study also supports the limited Fe/Mn intermixing in our system.

In Fig. 10, we compare the remanent MOKE signal, which is also the saturation signal due to the square loops, of n ML Fe on $Cu_3Au(100)$ and 15 ML Mn/$Cu_3Au(100)$. Because of the same MOKE geometry and Fe crystalline structure (bcc), the comparison provides the information about the "dead layer" of Fe film, which is nonferromagnetic due to Fe-Mn intermixing at the interface or the possible AFM fcc Fe. Figure 10 clearly exhibits that the dead layer of Fe is only about ~2 ML, which is consistent with the AES data in Fig. 9. Such thin dead layer is not enough to provide the exchange bias with blocking temperature near RT. (In the previous studies,[27–29] 9–10 ML FeMn is needed to have blocking temperature near 300 K.)

Besides, the MOKE measurement of 21 ML Fe/n ML Mn/$Cu_3Au(100)$ is also performed, as shown in Fig. 11. For both RT- and LT-Mn, the T_b and H_e become smaller with thinner Mn layer, since the formations of fcc Fe and thin FeMn alloy are strongly correlated to the condition of the Fe/Mn interface, not to the total Mn thickness. If the FM/AFM coupling comes from the fcc Fe or thin FeMn alloy films, Mn thickness will not result in such a strong effect on the H_e and T_b. Therefore, the AFM is concluded to come from the Mn film, rather than the fcc Fe or thin FeMn alloy films near the Fe/Mn interface.

As mentioned in Sec. III A, the AES results reveal that significant Mn-Cu-Au alloying may extend to only 1–2 ML near the interface. In the x-ray magnetic circular dichroism studies of Huttel *et al.*,[30] a $c(2\times2)$MnCu(100) surface prepared by 0.5 ML Mn/Cu(100) reveals long-range magnetic ordering with T_C=50 K. In our MOKE measurement, no hysteresis loop was observed in n ML Mn/$Cu_3Au(100)$ at

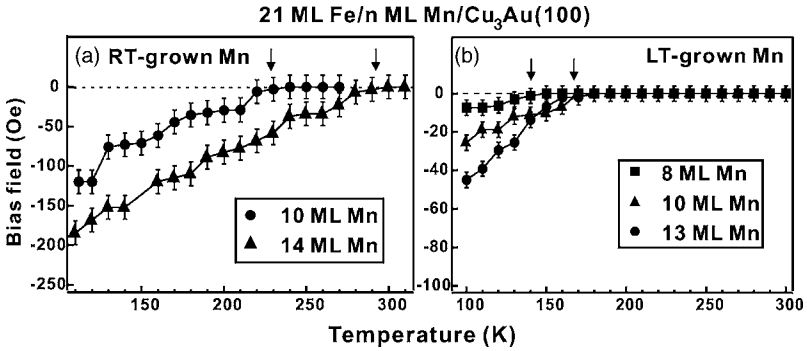

FIG. 11. (a) and (b) show the exchange bias field of the 21 ML Fe/n ML RT- and LT-grown Mn bilayers on $Cu_3Au(100)$ as functions of temperatures. The arrows indicate the critical temperatures for the disappearance of exchange bias, the so-called blocking temperature T_b. These results exhibit that both the growth temperature and the Mn film thickness affect the exchange bias field significantly.

110–300 K, indicating the absence of ferromagnetic MnCu alloy interface layers at the measurement temperature. As shown in Fig. 12, the monotonic increase of bias field (H_e) in Fe/8–15 ML RT-Mn and Fe/8–13 ML LT-Mn also contradicts the decaying behavior of Ruderman-Kittel-Kasuya-Yosida (RKKY) coupling,[31,32] indicating the very minor effect from the possible FM or AFM alloy interface layers with RKKY coupling.

The 21 ML Fe/Mn bilayers with higher Mn thickness up to 20–30 ML are also prepared. The enhanced coercivity is also observed in these bilayers, indicating the existence of exchange bias coupling. However, since as shown in Fig. 11 the blocking temperature of 21 ML Fe/14 ML Mn is close to RT, for 21 ML Fe/20–30 ML Mn we need to perform the field-cooling process from temperature much higher than RT in order to observe the bias field. Such high-temperature annealing might lead to more serious interdiffusion at the interfaces and might create more complexities. That is why the data of RT-Mn above 15 ML are not shown in Figs. 11 and 12.

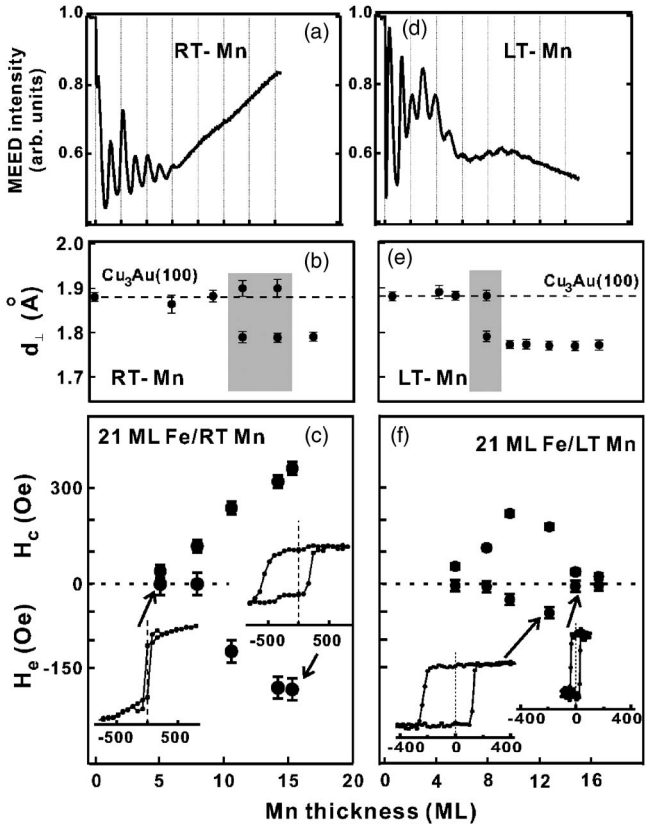

FIG. 12. The summarized results of [(a) and (d)] the growth (MEED) and [(b) and (e)] the crystalline structure ($d_\perp$) for RT- and LT-grown Mn films as functions of thickness. The magnetic properties (H_c and H_e) for (c) 21 ML Fe/RT-grown Mn/$Cu_3Au(100)$ and (d) 21 ML Fe/LT-grown Mn/$Cu_3Au(100)$ as functions of Mn film thickness. All the data were measured from the MOKE hysteresis loops at 100 K. The insets show the MOKE hysteresis loops of the indicated data points. The x-axis of the insets is the magnetic field with the unit of Oe.

Figures 12(c) and 12(f) summarize the H_c and H_e of Fe/RT-Mn and Fe/LT-Mn bilayers measured at 110 K as functions of Mn thickness. The insets give examples of the hysteresis loops with or without the FM/AFM exchange bias coupling. For RT-Mn, the H_c and H_e monotonously increase with Mn thickness up to 15 ML. This result is reasonable considering the finite-size effect. The higher thickness means higher T_N and stronger AFM properties, which result in the larger H_c and H_e.[33] For LT-Mn, initially the H_e and H_c increase with thickness and reach the maximum at ~13 ML. However, after ~15 ML, the H_c drastically decreases and the H_e disappears. It indicates the absence of exchange bias coupling in the Fe/LT-Mn bilayers with Mn thickness >15 ML. Just like the case of RT-Mn, the increase of H_e and H_c in the low coverage region is related to the finite-size effect. However, the morphology of LT-Mn films becomes rougher and rougher with increasing thickness. The enhanced roughness strongly reduces the exchange bias coupling. Thus, after 15 ML, the features of exchange bias coupling, including the bias field and the enhanced H_c,[33] disappear.

In a short summary, significant exchange bias coupling is observed in Fe/RT-Mn bilayers. The exchange bias coupling in Fe/LT-Mn is much weaker than that in Fe/RT-Mn and drastically varies with film thickness. The presence of exchange bias in the Fe/Mn bilayers also indicates the antiferromagnetism of γ-phase Mn/$Cu_3Au(100)$.

IV. DISCUSSION

A. fcc and fct structures of Mn films

From the analysis of LEED patterns and LEED-I/V curves, both the RT- and LT-Mn films reveal a fcc to fct structural transition with increasing thickness. The atomic volumes (V) and tetragonal distortion ratios (c/a) are $V=13.3$ and 12.4 Å^3 and $c/a=1.01$ and 0.95 for fcc and fct structures,[34] respectively. For comparison, the structural in-

TABLE I. The atomic volumes and tetragonal distortion ratios c/a of bcc and fct Mn films on different substrates as well as the alloyed bulk γ-Mn.

Substrate	Alloyed bulk γ-Mn[a]	$Cu_3Au(100)$[b]	Co/Cu(100)[c]	Ag(100)[d]	Fe(100)[e]	Pd(100)[f]
V (Å^3)	12.94	13.3(fcc), 12.4(fct)	12.46	13.8	13.5	13
c/a	0.946	1.01(fcc), 0.95(fct)	1.055	0.81	0.81	0.88

[a]Reference 2.
[b]Reference 34.
[c]Reference 35.
[d]Reference 7.
[e]Reference 6.
[f]Reference 36.

formation of Mn films epitaxially grown on 20 ML Co/Cu(100),[35] Ag(100),[7] Fe(100),[6] and Pd(100)[36] are summarized in Table I. In the studies of Schirmer *et al.*,[12] 5.2 and 16 ML $Mn/Cu_3Au(100)$ films (grown at 173 K) were investigated by dynamic LEED calculation. Our results are the same as theirs within the errors. Moreover, our studies not only reveal the consistent structural information but also clarify the detailed critical thickness for fcc-fct transition with different growth temperatures. Besides, alloyed bulk γ-Mn can be prepared by rapid quenching, revealing a (100) layer-by-layer antiferromagnet with the Néel temperature of 540 K. By extrapolating the lattice constants of alloys to zero concentration of impurity, the crystalline structure of pure γ-Mn can be estimated as $a=3.796$ Å, $c=3.592$ Å, $V=12.94$ Å^3, and $c/a=0.946$, very close to the results of $Mn/Cu_3Au(100)$. As compared with other systems listed in Table I, $Cu_3Au(100)$ is very unique in sustaining the pure γ-Mn up to more than 30 ML (see Fig. 5). The main reason might come from the small lattice misfit between γ-Mn and $Cu_3Au(100)$. In addition to these experimental studies, theoretical calculations[11] on Mn also show an AFM equilibrium state at $c/a=0.96$. The significant exchange bias coupling of Fe/Mn bilayers shown in Figs. 8 and 9 confirms the AFM state of pure γ-Mn, in agreement with the alloyed bulk γ-Mn and the theoretical calculation. Furthermore, the roughness-induced disappearance of exchange bias in Fe/LT-Mn bilayers (Fig. 10) might also provide the indirect evidences for the (100) layer-by-layer AFM structure in pure γ-Mn.

About the fcc-fct structural transition, it is interesting to ask why the LT growth advances the critical thickness from 12–14 to ~8 ML as compared with RT growth. Up to now, no conclusive prediction is given in theory and the experimental results are also diverse. For example, LT growth of $Fe/Cu_3A(100)$ delays the fcc-bcc structural transition to 5.5 ML as compared with the critical thickness of 3.5 ML for RT growth.[14,15] In contrast, as shown in this work, LT growth of $Mn/Cu_3Au(100)$ advances the fcc-fct structural transition to 8 ML as compared with the higher critical thickness of 12–14 ML for RT growth. Therefore, the growth-temperature effect on the structural transition in ultrathin films is quite complicated and drastically varies with the different systems. For the present case of $Mn/Cu_3Au(100)$, the following possibilities are proposed. LT growth usually enhances the roughness, which also means the enhancement of island, defect, and dislocation densities, and thus easily triggers the structural transition at lower thickness. In the LT-Mn films, given the larger roughness of these layers, which will most likely grow in the form of pyramids, the upper atomic levels of these islands will become occupied much earlier than in the flatter, RT-Mn films. Thus, the influence of the substrate template will be lost at an earlier stage of growth, and the top of the islands might start relaxing sooner.

From the studies of LEED patterns and LEED-I/V curves shown in the above sections, the fcc and fct Mn films reveal the different values of volume per atom: 13.3 ± 0.4 and 12.4 ± 0.4 Å^3, respectively.[34] As mentioned in Sec. III A, Au-segregation is observed in RT-grown Mn films. Similar phenomenon is also observed in Ni films grown on the same substrate $Cu_3Au(100)$. Since the size of Au atom is larger than Mn, the segregation may help sustain the structure of the larger atomic volume: the fcc structure. However, if we also consider the Cu segregation, since the Cu atom size is smaller than Mn, the above deduction may not be necessarily true. It is difficult to conclude if the Cu- and Au-segregation effects prefer delaying or advancing the fcc-fct transition.

Although both the theoretical calculation[11] and experimental results[12,13] already show the fct structure to be the ground (most stable) state for AFM γ-phase Mn, it is still worth asking why the fcc structure exists in low thickness regions (<8 ML for RT-Mn, <12 ML for LT-Mn). One reason might come from the substrate effect. The epitaxial films usually reveal similar crystalline structure as the substrate with low thickness, for example, the fcc-Fe films on fcc-Cu(100) or fcc-$Cu_3Au(100)$ substrates, although bulk Fe is of bcc structure. Besides, it should be noticed that the theoretical calculations also indicate the fcc structure ($c/a=1$) to be the most stable state in nonmagnetic (NM) γ-phase Mn.[11] In ultrathin films, due to the finite-size effect, which comes from the limited thickness and the symmetry breaking on the surface and interface, the T_N is significantly reduced with the decreasing thickness. The T_b of Fe/Mn exchange bias coupling shown in Fig. 11 also infers that T_N of low thickness Mn films might range to lower than 300 K. It is known that when above or near T_N, the thermal energy is high enough to overcome the energy difference between the AFM and NM states. Accordingly, at such growth temperatures compatible with T_N, it is difficult to tell which of the fct-AFM phase or the fcc-NM phase is stable. It also might be one of the reasons why the fcc-fct structural transition is easily tuned by growth temperature.

B. Origin of plaid pattern in RT-Mn

In the STM studies, a plaid pattern is observed in the surface morphology of RT-grown $Mn/Cu_3Au(100)$ with the thickness ≥ 14 ML. The grid lines of this plaid pattern are not very straight, but roughly along the $\langle 010 \rangle$ directions. Since the periodicity is not regular ($\sim 10-20$ nm), the LEED images shown in Fig. 2 do not reveal any information about the plaid pattern. From the line profile shown in the insets of Fig. 6, the height of the grid lines is less than 1 Å. It indicates not that this pattern is composed of additional atoms on the flat terraces but that the grid might be some kind of defect or dislocation. Accordingly, the grid lines follow and continue even across the step between two different terraces [Fig. 6(h)].

Since the pattern appears right at the thickness region of the fcc-fct structural transition, the grid might be the defects or dislocations induced by the structural transition. In the case of 6.2 ML LT-$Fe/Cu_3Au(100)$,[14] a similar networklike fine structure with nearly square units is also observed on the closed film. Upon a more detailed analysis, the nearly square units have heights of ~ 0.15 Å and sides of $7-14$ Å. Interestingly, in the LT-$Fe/Cu_3Au(100)$ system, the appearance of the networklike structure is also at the same critical thickness as the fcc-bcc structural transition (~ 6 ML). It strongly implies the connection between the networklike structure and the structural transition. For the case of $Mn/Cu_3Au(100)$, the lattice mismatch between the Cu_3Au and the bulk γ-phase Mn-rich alloys ranges from 1.1% to −1.9%. The projection of the nearest-neighbor length in the $\langle 001 \rangle$ directions is ~ 1.88 Å. If during the fcc-fct transition the in-plane relaxation of $\sim 1\%$ is triggered, then the average length needed to release the strain will be $1/(1\%) \times 1.88\ \text{Å} \approx 20$ nm, which is roughly consistent with the size of the grid. Due to the finite size of the LEED spots, the possible relaxation in lateral lattice within 1% is difficult to observe from the analysis of LEED images. Therefore, no direct evidence can prove if the in-plane relaxation within 1% truly happens. Eventually, it can be concluded that the plaid pattern is connected to the onset of fcc-fct structural transition. Meanwhile, the possibility of the in-plane relaxation within 1% cannot be excluded.

C. Interrelations between magnetism, structure, and interface roughness

Since both the RT-grown and LT-grown Mn films reveal a fcc-fct structural transition, the following question arises: Does the structure transition connect to any change in magnetic properties? The summarized data of growth (MEED), crystalline structure ($d_\perp$), and magnetic properties (H_c and H_e) are shown in Fig. 12. The monotonic increase of H_e and H_c in low coverage region for both RT- and LT-Mn is related to the finite-size effect. The higher thickness means higher T_N and stronger AFM properties, and thus results in the larger H_c and H_e.

It is interesting to observe that the onset of Fe/Mn exchange bias coincides with the critical thickness of the structural transition [Figs. 12(b), 12(c), 12(e), and 12(f)]. Thus, there seems to be some correlation between the structural transition and magnetic properties. However, the possibilities of finite-size effect or roughness effect still cannot be excluded. The direct measurements of AFM γ-Mn films by x-ray magnetic linear dichroism[37] and spin-polarized STM (Refs. 38 and 39) are also ongoing for the more detailed information about the spin configuration.

In another aspect, from the MEED oscillation curves of LT-Mn on $Cu_3Au(100)$ and the growth condition of the subsequent Fe layers on $Mn/Cu_3Au(100)$ shown in Fig. 7, we can conclude there is a smooth surface for RT-Mn and a rough surface for LT-Mn in the high thickness region (after ~ 10 ML). From the comparison between RT- and LT-Mn MEED curves, the roughness of $6-10$ ML LT-Mn is similar to that of RT-Mn. However, after 10 ML, the roughness of LT-Mn is getting worse, and meanwhile RT-Mn film is getting smoother and smoother. This also might be why we get such dramatic changes in H_c and H_e after ~ 10 ML(Fig. 12) for LT-Mn. Besides, the fcc structure transforms into the fct structure through relaxation of the interlayer spacing along the c-axis (normal to the surface). It maintains the highest crystal symmetry and does not necessarily induce roughness. Thus, although the fcc-fct structural transition of LT-Mn happens at 8 ML, the surface morphology is not necessarily getting worse at the same time. Also in the STM results of RT-Mn (Fig. 6), the fcc-fct structural transition does not have significant effect on roughness.

In the previous studies, a layered (100) AFM structure of γ-Mn has been predicted by theoretical calculation[40] and measured in a study of γ-FeMn and extrapolation to zero Fe content.[2] In this Fe/γ-Mn bilayer system, the significant exchange bias field and the strong correlation between H_e and surface morphology also indicate the possibility of the (100)-layered AFM structure of the γ-Mn films. For such uncompensated layered AFM structure, the roughness creates areas of different spin orientations; thus the total number of spin pinning the FM in one direction usually will be reduced.[41] Besides, we need to note that there are some experiments and models that indeed reveal the increasing exchange bias with roughness.[42,43] However, in general, the roughness-enhanced exchange bias is observed in compensated AFM structures.[44–46] In these cases, the roughness may induce local areas with net spin moment, so that the exchange bias may be increased by increasing the roughness. On the other hand, in the case of single-crystalline (001)-layered AFM structure for γ-Mn, it is very possible for the roughness to decrease the exchange bias since it creates areas of different spin orientations.[41] We need to agree that the roughness-induced reduction of exchange bias in Fe/LT-Mn is an indirect deduction. However, based on our detailed experimental results, as well as the previous calculations[40] and experiments[2] on γ-Mn, this γ-$Mn/Cu_3Au(100)$ system is very likely to be (100)-layered AFM structure, and the interface roughness can easily reduce the exchange bias coupling in such layered AFM structure.

V. SUMMARY

$Mn/Cu_3Au(100)$ films deposited at RT and LT are shown to reveal very different behaviors in the morphology, crystal-

line structure, and magnetism. The following comparisons and conclusions are made.

(1) From MEED and STM data, RT-Mn films exhibit smooth morphology composed of large terraces at high coverage. An interesting plaid pattern is observed on the RT-Mn surface. It should be connected to the structural transition or relaxation. The LT-Mn films reveal a layer-by-layer growth for 0–5 ML followed by reduced oscillations and decreasing MEED intensity, indicating the rough surface. The growth condition of the Fe overlayer also suggests the rough surface in LT-Mn films.

(2) Both the RT- and LT-Mn films exhibit a fcc-fct structural transition, but at different critical thicknesses, ~12–14 and ~8 ML, respectively. From LEED, the LT-Mn and RT-Mn films always sustain the coherent growth even after the fcc-fct transition.

(3) Significant exchange bias is observed in Fe/RT-Mn bilayers and monotonously increases with Mn thickness. The exchange bias coupling in Fe/LT-Mn is much weaker than that in Fe/RT-Mn and drastically varies with Mn film thickness due to the enhanced roughness in LT-grown films. The presence of exchange bias in the Fe/Mn bilayers also indicates the antiferromagnetism of γ-phase Mn/Cu_3Au(100).

ACKNOWLEDGMENTS

This work was supported by the National Science Council of Taiwan under Grant Nos. NSC 94-2112-M-002-005, NSC 95-2112-M-002-051-MY3, and NSC 94-2112-M-001-045 as well as the National Nano program under Grant No. NSC 95-2120-M-002-015.

*Corresponding author. Email address: mtlin@phys.ntu.edu.tw

[1] D. Hobbs, J. Hafner, and D. Spišák, Phys. Rev. B **68**, 014407 (2003).
[2] Yasuo Endoh and Yoshikazu Ishikawa, J. Phys. Soc. Jpn. **30**, 1614 (1971).
[3] J. T. Kohlhepp and W. J. M. de Jonge, J. Appl. Phys. **95**, 6840 (2004).
[4] W. Pan, R. Popescu, H. L. Meyerheim, D. Sander, O. Robach, S. Ferrer, Minn-Tsong Lin, and J. Kirschner, Phys. Rev. B **71**, 174439 (2005).
[5] W. Pan, D. Sander, Minn-Tsong Lin, and J. Kirschner, Phys. Rev. B **68**, 224419 (2003).
[6] S. Andrieu, M. Finazzi, P. Bauer, H. Fischer, P. Lefevre, A. Traverse, K. Hricovini, G. Krill, and M. Piecuch, Phys. Rev. B **57**, 1985 (1998).
[7] B. T. Jonker, J. J. Krebs, and G. A. Prinz, Phys. Rev. B **39**, 1399 (1989).
[8] S. L. Qiu and P. M. Marcus, Phys. Rev. B **60**, 14533 (1999).
[9] S. L. Qiu, P. M. Marcus, and Hong Ma, Phys. Rev. B **62**, 3292 (2000).
[10] T. Oguchi and A. J. Freeman, J. Magn. Magn. Mater. **46**, L1 (1984).
[11] P. Krüger, O. Elmouhssine, C. Demangeat, and J. C. Parlebas, Phys. Rev. B **54**, 6393 (1996).
[12] B. Schirmer, B. Feldmann, A. Sokoll, Y. Gauthier, and M. Wuttig, Phys. Rev. B **60**, 5895 (1999).
[13] W. C. Lin, L. C. Lin, T. Y. Chen, B. Y. Wang, Ker-Jar Song, and Minn-Tsong Lin, J. Appl. Phys. **97**, 10K112 (2005).
[14] M.-T. Lin, J. Shen, W. Kuch, H. Jenniches, M. Klaua, C. M. Schneider, and J. Kirschner, Surf. Sci. **410**, 290 (1998).
[15] M.-T. Lin, J. Shen, W. Kuch, H. Jenniches, M. Klaua, C. M. Schneider, and J. Kirschner, Phys. Rev. B **55**, 5886 (1997).
[16] M. Zheng, J. Shen, P. Ohresser, Ch. V. Moha, M. Klaua, J. Barthel, and J. Kirschner, J. Appl. Phys. **85**, 5060 (1999).
[17] S. Muller, P. Bayer, C. Reischl, K. Heinz, B. Feldmann, H. Zillgen, and M. Wuttig, Phys. Rev. Lett. **74**, 765 (1995).
[18] B. Y. Wang, W. C. Lin, Y. W. Liao, Ker-Jar Song, and Minn-Tsong Lin, Surf. Sci. **600**, 4517 (2006).
[19] C. C. Kuo, C. L. Qiu, W. C. Lin, and Minn-Tsong Lin, Surf. Sci. **520**, 121 (2002).
[20] C. C. Kuo, W. C. Lin, C. L. Qiu, H. L. Huang, and Minn-Tsong Lin, J. Appl. Phys. **89**, 7153 (2001).
[21] W. C. Lin, B. Y. Wang, Y. W. Liao, Ker-Jar Song, and Minn-Tsong Lin, Phys. Rev. B **71**, 184413 (2005).
[22] W. C. Lin, C. C. Kuo, C. L. Chiu, and M.-T. Lin, Surf. Sci. **478**, 9 (2001).
[23] F. Matthes, M. Seider, and C. M. Schneider, J. Appl. Phys. **91**, 8144 (2002).
[24] K. L. Man, W. L. Ling, Silena Y. Paik, H. Poppa, M. S. Altman, and Z. Q. Qiu, Phys. Rev. B **65**, 024409 (2001).
[25] A. Braun, B. Feldmann, and M. Wuttig, J. Magn. Magn. Mater. **171**, 16 (1997).
[26] T. K. Yamada, M. M. J. Bischoff, T. Mizoguchi, and H. van Kempen, Surf. Sci. **516**, 179 (2002).
[27] F. Offi, W. Kuch, and J. Kirschner, Phys. Rev. B **66**, 064419 (2002).
[28] R. Thamankar, S. Bhagwat, and F. O. Schumann, Phys. Rev. B **69**, 054419 (2004).
[29] R. Thamankar, S. Bhagwat, and F. O. Schumann, Phys. Rev. B **69**, 054411 (2004).
[30] Y. Huttel, C. M. Teodorescu, F. Bertran, and G. Krill, Phys. Rev. B **64**, 094405 (2001).
[31] N. J. Gökemeijer, T. Ambrose, and C. L. Chien, Phys. Rev. Lett. **79**, 4270 (1997).
[32] Minn-Tsong Lin, C. H. Ho, C. R. Chang, and Y. D. Yao, Phys. Rev. B **63**, 100404(R) (2001).
[33] W. Pan, N. Y. Jih, C. C. Kuo, and Minn-Tsong Lin, J. Appl. Phys. **95**, 7297 (2004).
[34] The lateral and perpendicular lattice constants are determined by LEED and LEED-I/V with an error of ±1%, and thus the error in determining the volume per atom is ±3%.
[35] J. T. Kohlhepp and W. J. M. de Jonge, Phys. Rev. Lett. **96**, 237201 (2006).
[36] S. W. D. Tian, F. Jona, and P. M. Marcus, Solid State Commun. **70**, 199 (1989).
[37] C. Grazioli, Dario Alfè, S. R. Krishnakumar, Subhra Sen Gupta, M. Veronese, S. Turchini, Nicola Bonini, Andrea Dal Corso, D. D. Sarma, Stefano Baroni, and C. Carbone, Phys. Rev. Lett. **95**,

117201 (2005).
[38] T. K. Yamada, M. M. J. Bischoff, G. M. M. Heijnen, T. Mizoguchi, and H. van Kempen, Phys. Rev. Lett. **90**, 056803 (2003).
[39] U. Schlickum, N. Janke-Gilman, W. Wulfhekel, and J. Kirschner, Phys. Rev. Lett. **92**, 107203 (2004).
[40] J. Hafner and D. Spišák, Phys. Rev. B **72**, 144420 (2005).
[41] J. Nogués and Ivan K. Schuller, J. Magn. Magn. Mater. **192**, 203 (1999).
[42] Miguel Kiwi, J. Magn. Magn. Mater. **234**, 584 (2001).
[43] T. J. Moran, J. M. Gallego, and Ivan K. Schuller, J. Appl. Phys. **78**, 1887 (1995).
[44] T. C. Schulthess and W. H. Butler, Phys. Rev. Lett. **81**, 4516 (1998).
[45] T. C. Schulthess and W. H. Butler, J. Appl. Phys. **85**, 5510 (1999).
[46] J. R. L. de Almeida and S. M. Rezende, Phys. Rev. B **65**, 092412 (2002).